International Journal of Recent Technology and Engineering (IJRTE)
ISSN: 2277-3878 (Online), Volume-8 Issue-2, July 2019

Proper Orthogonal Decomposition of a Very High Concentrated Release of Sediment in Water: Spatio Temporal Patterns

Duc Hau Nguyen, Sylvain Guillou, Le Thi Thu Hien, Quang Hung Nguyen

Abstract*: Proper Orthogonal Decomposition (POD) is based on a space and time decomposition and on the finding of eigenfunctions. It is a technique for recognizing or identifying key dominant features in data sets. The release of high sand concentrated in water induces a flow with particular structures as showed experimentally by Villaret et al. [1]. Two-phase flow simulations with no current were presented by Guillou et al. [2]. The present paper shows the POD-analyses of results of such a simulation with and without current. Two spatio-temporal fields, the solid volume fraction and the solid phase velocity within the sediment release coherent structures are successfully captured by applying Proper Orthogonal Decomposition on numerical simulation results..

Keywords*: Dredged sediment release, sediment transport, two-phase flow modelling, fine sand, snapshot proper orthogonal decomposition (POD)..

I. INTRODUCTION

The port structures are often established in areas where water levels are fairly low, especially in estuaries. It is then necessary to perform dredging to allow ships accessing to the docks. The dredged sediment is released over a predefined deposit zone. Because of the concentration of the sediment cloud appearing during the release, more than 350 g/l at the beginning, there is an impact on the environment. After the release, the sediments settle under a cloud of very high concentration. This settling step is followed after impact on the bed by the formation of turbidity current. Due to the high concentrated fluid-solid mixture the use of a two-phase flow model to simulate the three different steps of the phenomenon is recommended.

Guillou et al. [2] applied the two-phase flows model (NSMP-code) developed by Barbry et al. [3, 4] to the sand release in a channel corresponding to the experiments of Villaret et al. [1] in the no-current case. The different steps of the flow observed by Villaret et al.[1] are simulated. More simulations were performed by Nguyen et al.[5], especially, in the case of release with a lateral current in the channel. The motions of very high concentrated releases are studied by considering with different values of the current.

Proper Orthogonal Decomposition (POD), known as Principal Component Analysis and Karhunen-Loeve Decomposition, is a technique which allows the identification of the coherent structures in turbulent fluid flows that contribute most to the energy. It is based on a space and time decomposition on the finding of eigenvalues and extracts a spatial dependent orthonormal basis functions and time dependent orthogonal time functions from a dynamic system. These basis are optimal for the reconstruction of a set of flow samples and are characteristic of the most probable flow realizations (cf. Holmes et al. [6]).

The snapshot POD method [7] is particularly well adapted to the analysis of simulation's results. It was used by Cizmas et al.[8] to analyse the spatio-temporal pattern in fluidized beds. They analyzed the numerical simulations results of the hydrodynamics of a fluidized bed to obtain a reduced order model of the interaction between the gas and the solid particles. Yuan et al. [9] used it for bubbling fluidized bed, and Brenner et al. [10] used it for unsteady gas flows or bubbles in multiphase flow. POD technique can lead to the information extraction from experimental and numerical data and thus to a quantitative comparison between results for validation purposes. Moreover, variables as solid volume fraction can not be easily obtained by the experimental way. However, in this paper, the purpose is to study the merits of snapshot POD technique on the mud release phenomenon. Results obtained with the NSMP-code [4, 5] for different current velocities and particle sizes are considered. Spatial dominant features are identified and separated from the spatio-temporal dynamics of the simulations.

In the following section release phenomenon and the numerical set up are introduced. In section 3 this paper recalls the well-known Proper Orthogonal Decomposition and more particularly the Snapshot POD. Results obtained for a mud release without ambient current for two different kind of sand are provided in section 4. The impact of the ambient current is explained on section 5 and finally discussions and conclusions are given in section 6.

Revised Manuscript Received on 30 July 2019.
***** Correspondence Author

Duc Hau Nguyen*, Thuyloi University, Hanoi, 100000 Ha noi, Vietnam. **Sylvain Guiolou,** Laboratoire Universitaire des Sciences Appliquées de Cherbourg (EA4253), Université de Caen. Site Universitaire de Cherbourg, BP 78, 50130 Cherbourg-Octeville, France

Le Thi Thu Hien, Thuyloi University, Hanoi, 100000 Ha noi, Vietnam.

Quang Hung Nguyen, Thuyloi University, Hanoi, 100000 Ha noi, Vietnam.

II. EXPERIMENTAL AND MODELLING CONFIGURATION

A. The release phenomenon

Laboratory experiments of sand release have been developed and described by Villaret et al. [1]. These experiments were performed in a straight channel of 72 *m* long, of 1.5 *m* wide and of 1.5 *m* height. A specifically designed recipient (maximum capacity of 60 litters) is placed at 15 *cm* below the free-water surface. The ambient current is imposed by a hydraulic pump. Then the sand-water mixture is filled-up in the recipient at a given concentration. Finally, the bottom of recipient is suddenly opened (Figure 1b) and the measurement (photo-camera and concentration) starts simultaneously.

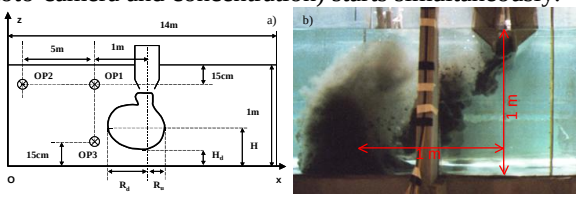

Fig. 1. Definition sketch of the release phenomenon: a) location of optical sensors (OP) for turbidity measurements; b) mud dumping [3]

B. Governing equations and configurations studied

The two-phase flow model (NSMP-code) is based on the Eulerian-Eulerian (or two-fluid) description. The model is fully described in [4, 5]. Herein we briefly recall the basic equations with special closures for the sediment dumping case. The governing equations (1) are written for each phase. The subscript *k* could be "*f*" for fluid and "*s*" for solid phase:

$$\begin{cases} \dfrac{\partial(\alpha_k)}{\partial t} + \vec{\nabla}\cdot\left(\alpha_k \vec{u}_k\right) = 0 \\ \dfrac{\partial\left(\alpha_k \vec{u}_k\right)}{\partial t} + \vec{\nabla}\cdot\left(\alpha_k \rho_k \vec{u}_k \otimes \vec{u}_k\right) = \dfrac{1}{\rho_k}\vec{\nabla}\cdot\left(\alpha_k\left(-p_k \bar{\bar{I}} + \bar{\bar{\tau}}_k + \bar{\bar{\tau}}_k^{\mathrm{Re}}\right)\right) + \alpha_k \vec{g} + \dfrac{1}{\rho_k}\vec{M}_k \end{cases} \quad (1)$$

where α_k, $\vec{u}_k$ and ρ_k stand for the volume fraction, velocity and density of phase *k* respectively, $\vec{g}$ is the acceleration of gravity, M_k the inter-phase momentum transfer, p_k the pressure of phase *k*, $\bar{\bar{\tau}}_k$ (or $\bar{\bar{\tau}}_k^{\mathrm{Re}}$) the viscous (or Reynolds, respectively) stress tensor. The sum of volume fractions, α_k, is obviously equal to 1. In this model, the viscous stress tensor is considered as a function of shear-stress tensors. It is worth noting that viscosity coefficients used for the solid stress are weighted by an amplification factor β, which accounts for the non-Newtonian behaviour of sediment flows. This is depending on the inter-particle distance, which depends itself on the maximum volume fraction $\alpha_{s,\max}$ (close to the packing concentration, whose value is equal to 0.625 for non-cohesive spherical and mono-dispersed solid particles). Different turbulent closures are available in the present version of the code. For more information about the presentation of the equations of the numerical technique refers to Nguyen et al. [4].

C. Studied Configurations

The 2-D X/Z computation domain extends over 14 *m* in the horizontal direction (positive upstream, centred to the dumping location) and over 1m on the vertical one. A regular mesh of 1401 nodes on the horizontal and 61 vertical nodes is used (14 m width x 1m height), the time step were fixed to 0.001s and the GMRES were selected. The lateral boundaries are considered as open and the bottom is impermeable. At the injection location (inlet diameter = 10 *cm*), the concentration and a Poiseuille parabolic profile of maximum velocity (W_{inj}) are imposed.

Tests		e11	e12	e13	e14	e15	e16	e17	e18	e19	e20
W_{inj} (m/s)		0.79	0.89	0.79	0.89	0.79	0.89	0.79	0.89	0.79	0.89
D_p (µm)		90	160	90	160	90	160	160	90	160	90
Vr (l)		60	60	60	60	60	60	60	60	60	60
Uc (cm/s)		0	0	10	10	20	20	15	15	25	25

Tab. 1. Testing conditions and nomenclature: W_{inj} is the injection velocity from the recipient, D_p the sediment particle diameter (90 µm or 160 µm), ρ the dry density of the solid (2650 kg/m^3), Cm is the concentration of the mixture (450 g/l), Vr the volume of dumped material (60 l), Uc the ambient velocity [1].

The testing conditions of the cases simulated and decomposed are described in the table 1. Two different kind of sand called sand 1 and 2 with a sediment particle diameter of *90 µm* and *160 µm* were tested. It can be noted that in the present work, the reference cases are cases e 11 and 12, without ambient velocity (Guillou et al. [2]).

III. PROPER ORTHOGONAL DECOMPOSITION

A. Theoretical aspects

Let us consider a set of deterministic uncorrelated flow realizations represented by $u(x,t_i)$, $i=1,\ldots,M$.

Note that in this work we will consider $u(x,t_i)$ as scalar functions. The observations $u(x,t_i)$ are parameterized by t_i, which represents times. From this ensemble of observations POD extracts the time independent orthonormal basis of eigenfunctions $\{\Phi_k(x)\}$ which maximises the projection of the scalar functions $u(x,t_i)$ in a mean square sense; in other words POD is optimal in the description of the energy flow sense.

Solving the POD problem can be reduced to obtaining the solutions of an integral eigenvalue problem:

$$\int_D R(x,y)\Phi(y)dy = \lambda\Phi(x)$$

Where R is the averaged correlation function $R(x,y) = \langle u(x,t_i)u^*(y,t_i)\rangle$.

This problem is mathematically equivalent to the following optimisation problem:

$$\max \frac{\langle (u,\Phi)^2 \rangle}{(\Phi,\Phi)}$$

Where (.,.) is the scalar product and <.> the ensemble average.

The fluctuating field can be projected onto the $\Phi_k(x)$ POD basis and can be reconstituted as following:

$$\tilde{u}(x,t_i) = \sum_{k=1}^{m} a_k(t_i)\Phi_k(x), \quad i = 1,....,M$$

The temporal coefficients are obtained from the projection of u onto the $\Phi_k(x)$ POD basis: $a_k(t_i) = (u(x,t_i),\Phi_k), \quad i = 1,....,M$.

It is well-known that according to the definition used to calculate the ensemble average, different approaches of the POD can be obtained (classical or direct method, snapshot, extended,…). More informations about the proper orthogonal decomposition properties are available in Holmes et al. [6].

B. Snapshot POD

In this study, the numerical data set, consist of a short time sequence of M instantaneous scalar fields with a high temporal resolution, uniformly sampled for discrete times. The spatial domain consists on a discrete spatial grid points. Thus the snapshot P.O.D. seems to be the best approach in our case. In this approach the ensemble average introduced is a spatial average. The correlation function is then a two points time correlation tensor $C(t,t')$. As explained by Holmes [6] the snapshot method is based on the fact that the data $u(x,t_i)$ and the eigenfunctions $\Phi_k(x)$, span the same linear space. Thus the eigenfunctions can be formulated as following

$$\Phi_k(x) = \sum_{i=1}^{M} v_i^k u(x,t_i), \quad k = 1,.....,M.$$

and the eigenvalues λ_k and eigenvectors v_i^k of the eigenvalue problem previously presented can be obtained from the solution of :

$Cv = \lambda v$, where v are the eigenvectors and C is defined as following:

$$[C_{ij}] = 1/M\left(u(x,t_i),u(x,t_j)\right).$$

The computational implementation of the snapshot POD is clearly described by Cizmas et al. [8].

C. Energy definitions

Because the P.O.D. is a decomposition of the dynamic model in a basis where the projection of the energy is optimal, a little number of modes (m) is required to reconstitute the scalar field in an accurate way. Each eigenvalue λ_k is the energy contained by each spatio-temporal mode. The total POD energy (E) is equal to the sum of all the eigenvalues obtained by the decomposition. The relative energy of each mode is the ratio of λ_k and E. The cumulated energy for the k first modes is equal to the sum of the k first relative energy modes.

IV. POD RESULTS FOR A MUD RELEASE WITHOUT AMBIENT CURRENT

In this section, POD will be applied to the fluctuating fields of solid volume fraction and solid phase velocities, noted respectively α_s, $\boldsymbol{u}_s$ and $\boldsymbol{w}_s$. Reference cases e11 and e12 present mud release without ambient current configurations for sand 1 and sand 2.

For each case a hundred time instantaneous snapshots have been decomposed and the time between two consecutive snapshots is equal to 0.1 s.

Guillou et al. [2] studied the evolution of the sediment cloud as well as solid velocity fields in still water for both cases. It was observed that, the two-phase model reproduces two counter-rotating vortices, observed by experimental way by Villaret et al. [1], which allow a full development of the sediment cloud. As the cloud growths, the surrounding water is entering inside the cloud while the iso-value contour is expanding.

A. POD applied to the solid volume fraction

Figures 2 and 3 show the most energetic spatial eigenfunctions and temporal amplitude coefficients extracted by POD from 100 snapshots of solid volume fraction for the reference case e11. Results obtained from the decomposition of case e12 are not presented here. These 100 snapshots shows 10 s and concerns the three steps of the release phenomenon, the convective descent during which the sediment falls under the influence of gravity, the collapse occurring when the descending cloud or jet impacts the bottom dispersion, and the passive transport commencing when the sediment transport and spreading.

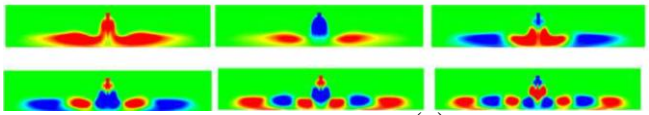

Fig. 2. POD spatial eigenfunctions $\Phi_k(x)$ obtained from the case e11 for the solid volume fraction (α_s). Positive values are colored in red, negative values are colored in blue.

As shown in Figure 2, the spatial eigenfunctions have a channel structure where the main flow motion is confined. The contribution of the eigenfunctions combined to the time amplitude coefficients introduces the fluctuating part of the phenomena.

As it can be observed in Figure 2, the first eigenfunction Φ_1 roughly represents a temporal average of the solid volume fraction fields during the mud release. It shows the occupying zone of the coherent structures during the interval of release decomposed.

So, this first eigenfunction present a symmetrical couple of coherent structures marked by the convective descent and the collapse of the descending cloud.

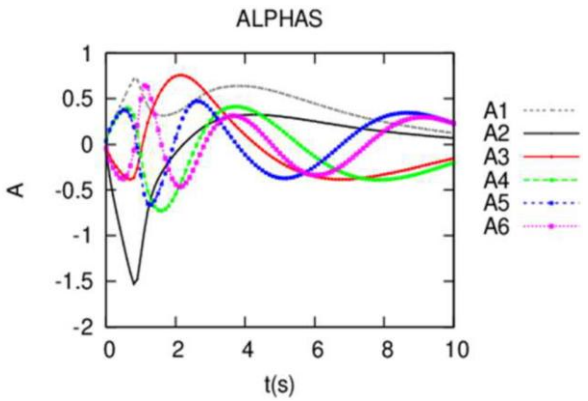

Fig. 3. Time evolution of POD amplitude coefficients obtained from the case e11.

As it can be observed in Figure 3, amplitude coefficients $a_1(t)$ present oscillations during the first seconds and after 2 s these are smoothed to lead to a constant value. The second eigenfunction Φ_2 shows two couples of coherent structures which seem to be linked to the convective descent and the collapse of the cloud.

Moreover the second amplitude coefficient $a_2(t)$ presents an important peak. Its maximum is close to 1 s. It can be reasonably supposed that this peak has a link to a characteristic time of physical phenomenon for example the convective descent time.

For increasing index of the eigenfunctions going from 3 to 8, coherent structures have also a symmetrical distribution and their size decreases. They present coherent structures with alternative positive and negative values. These structures present compact and regular form. The other amplitude coefficients have a more marked fluctuating behaviour, implying their contribution on the progressive passive transport of the sediment during the mud release.

About results obtained for case e12 (not presented here), Φ_1 and Φ_2 present only some differences compared to case e11. However the convective descent and the collapse of the cloud are also present in both eigenfunctions. The temporal evolution of the amplitude coefficients presents marked similarities between the cases e11 and e12.

For both reference cases eigenfunctions and amplitude coefficients reveal some well-defined coherent structures, which also support the existence of low-dimensional deterministic dynamics. Thus, these results reveal that the particle diameter has not a relevant impact on the spatial organization and temporal evolution of the solid volume fraction for release without ambient current.

B. POD applied to the solid phase velocities distributions

Figures 4 and 5 show the eigenfuctions and the amplitude coefficients obtained from the decomposition of the solid phase velocities fields ($\boldsymbol{u}_s$ and $\boldsymbol{w}_s$) for case e11.

As observed for the solid phase fraction the eigenfunctions show compact coherent structures with a symmetrical distribution and decreasing size with increasing index. All spatial eigenfunctions present couples of counter rotating coherent structures. Strong similarities are also observed between both cases e 11 and 12 (not presented here).

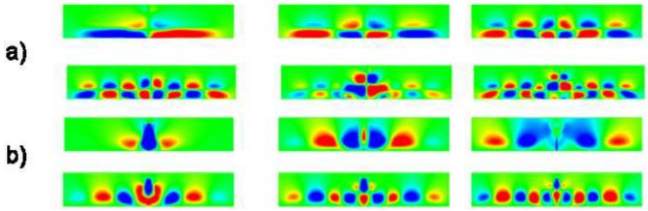

Fig. 4. POD spatial eigenfunctions $\{\Phi_k(\mathbf{x})\}$ obtained from the case e11 for the solid volume velocities: a) u_s and b) w_s.

Because of the snapshots decomposed concern the mud release the first eigenfunctions Φ_1 obtained for $\boldsymbol{u}_s$ and $\boldsymbol{w}_s$ are strongly linked to the mean velocities fields obtained during this instationary phenomenon. The convective descent seems to be also present for $\boldsymbol{w}_s$ in this eigenfunction (Φ_1).

Eigenfunctions and amplitude coefficients, with an index number superior to 1, are representative of the dynamics of the velocities fluctuations.

In one hand, for $\boldsymbol{u}_s$, Φ_2 seem to be linked to the dynamic collapse. In the other hand, for $\boldsymbol{w}_s$, coherent structures of Φ_2 seem to be linked to the convective descent.

For increasing index of the eigenfunctions going from 3 to 8, coherent structures have compact and regular form and seem to be linked to the progressive passive transport of the sediment during the mud release.

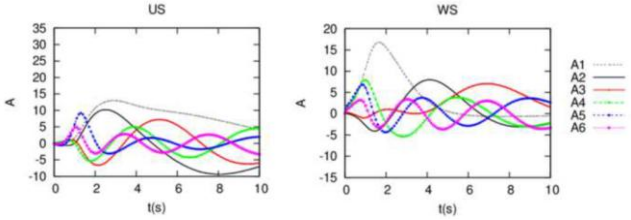

Fig. 5. Time evolution of POD amplitude coefficients obtained from the case e11.

Note that, these spatio-temporal modes present a marked spatial and temporal organization.

It can be also deduced that, in the same way that for solid volume fraction, particle diameter has not a relevant impact on the spatial organization and temporal evolution of the solid phase velocities, without ambient current.

V. IMPACT OF THE AMBIENT CURRENT

Spatial eigenfunctions and temporal amplitude coefficients will be shown in figures 6, 7 and 8 for POD applied to α_s, $\boldsymbol{u}_s$ and $\boldsymbol{w}_s$ for case e13, whose corresponds to the onset of the impact of the current ambient.

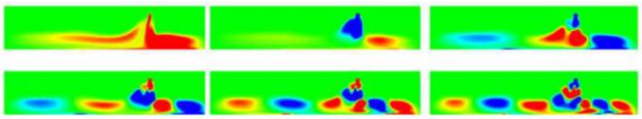

Fig.6. POD spatial eigenfunctions $\{\Phi_k(\mathbf{x})\}$ obtained from the case e13 for the solid volume fraction (α_s). Positive values are colored in red, negative values are colored in blue.

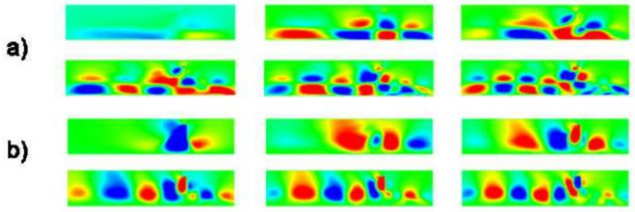

Fig. 7. POD spatial eigenfunctions $\{\Phi_k(\mathbf{x})\}$ obtained from the case e13 for the solid volume velocity : a) u_s and b) w_s.

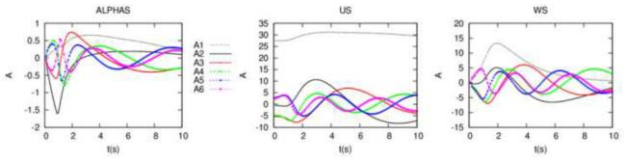

Fig. 8. Time evolution of POD amplitude coefficients obtained from the case e13 for the solid volume fraction (α_s) and the solid volume velocities (u_s and w_s.).

Figure 6 shows that for solid volume fraction α_s (case e13), ambient current (*Uc=10 cm/s*) presence break the symmetry of the coherent structures observed in the reference case e11. Moreover, this value of *Uc* has not a significant impact on the evolution of the amplitude coefficients (cf. figures 3 and 8).

Figure 9 illustrate Φ_1 for cases e 11, 13, 18, 15 and 20. It can be shown that the increasing value of *Uc* seem to imply that structures are less compact and their contour are less regular. Thus, it can be deduced that the increasing of *Uc* leads to a loss of the spatial organization of the solid volume fraction distribution.

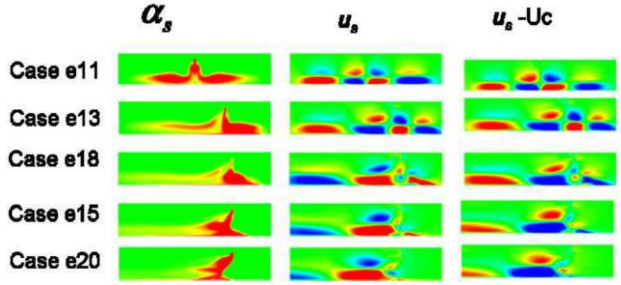

Fig. 9. POD spatial eigenfunction Φ_1 obtained from cases e11 to e20 for the solid volume fraction (α_s) and u_s-Uc. Positive values are colored in red, negative values are colored in blue.

In an opposite way, POD application on solid phase velocities distributions highlights that *Uc* has a marked impact on spatio-temporal modes. *Uc* has a notorious impact on the evolution of the most energetic temporal amplitude coefficients obtained from the decomposition of $\boldsymbol{u}_s$ snapshots. $a_1(t)$ is a constant value, close to 30, greater than the other amplitude coefficients. From eigenfunctions obtained from $\boldsymbol{u}_s$ and $\boldsymbol{w}_s$ decomposition, for index i>1, it can be concluded that spatial organization of structures is less coherent than in the reference cases. Indeed, near to the collapse zone, structures are not compact and have irregular contours. It can be supposed that heavy coherence losses can be observed for greater ambient velocities.

For case e13, with a little value of ambient current (*Uc)*, a complementary POD decomposition was applied on pretraited snapshots $\boldsymbol{u}_s$-*Uc*. Eigenfunction extracted (only Φ_1 is illustrated in figure 9) Φ_i is exactly the same, with possibly the opposite sign, than Φ_{i+1} obtained from the decomposition of $\boldsymbol{u}_s$ snapshots. About amplitude coefficients extracted from $\boldsymbol{u}_s$-*Uc*, $a_1(t)$ has identical evolution than $a_2(t)$ obtained from $\boldsymbol{u}_s$. For the other index we can observe, light differences.

The same equivalence is observed for cases e 18, 15 and 20 (cf. figure 9).

From the observation made for case e13 (with a little value of *Uc*=10 cm/s) different observations, it can be inferred that the ambient current has different impact on the spatio-temporal organization of the solid volume fraction and the solid phase velocities. In the first case, the impact is really light, in the second one the impact is clearly marked, and more particularly in eigenfunctions linked to the velocities fluctuations (index superior to 1).

As observed for α_s the enhancement of *Uc*, leads to a progressive loss of spatio-temporal organization of its dynamics for $\boldsymbol{u}_s$-*Uc*.

VI. ENERGETICAL ASPECT

Energetic data is listed in Table 2 and can be shown in figure 10.

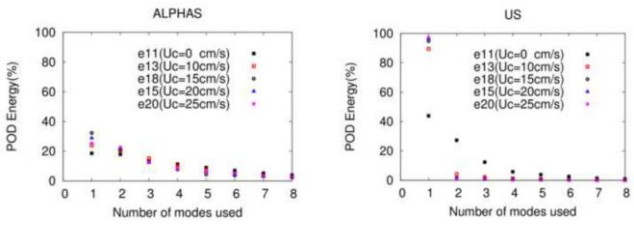

Fig. 10. Energy spectrums for the solid volume fraction and the solid phase velocity (u_s) for sand 1 cases.

A. POD applied to the solid volume fraction

For both references cases e11 and e12, it can be observed that 90% and 95% of E are respectively reached with the e9 and e13 most greater eigenvalues. Moreover the first eigenvalue λ_1 represents around 20% of the total energy E. Thus, for the solid volume fraction, it can be inferred that the first spatio-temporal mode has moderate impact on the dynamics (~20% of E).

However this is a complex dynamics, because the contribution of an important number of spatio-temporal modes is necessary to reach 95% of E and to obtain a good reconstitution of the solid volume fraction fields.

It can be inferred from figure 10, that the impact of the ambient current (varying from 0 up to 25 cm/s, cf. Table 1) on the POD energy spectrum obtained for α_s is not really significant. Indeed, it can be observed that for all cases studied for sand 1 the number of modes containing 90% or 95% does not change.

Thus, it can be concluded that, as observed for the spatio-temporal organization aspect, the ambient current has not an impact in the energetical aspect.

However, some modifications can be observed in the energy distributions (cf. Figure 10). Indeed, for the two first modes: the percentage of POD energy reaches a maximum of 33% for the case e18 compared to 19% obtained for e11 (*Uc=0 cm/s*). In other words, the distribution of the energy moves to the predominant modes.

As observed by Cizmas et al. [8] for fluidized beds it can be observed, for all *Uc* values, that solid volume fraction dynamics can be captures by a few POD eigenvalues.

B. POD applied to the solid phase velocities distributions

Note that, compared to the decomposition made for α_s less number of eigenvalues is necessary to reach the same percentage of E. For example, in the case of $\boldsymbol{u}_s$, 90% and 95% of E are respectively reached with the 4 and 6 eigenvalues. However, it can be also observed in table 2 that, for the reference cases (11 and 12) and both solid phase velocities ($\boldsymbol{u}_s$ and $\boldsymbol{w}_s$) λ_1 contains nearly 40% of E.

So, a strong coherent dynamics can not be rigorously concluded for the solid phase velocities.

	POD total energy and number of modes for the solid phase fraction α_s			
Case	Uc (cm/s)	$\lambda 1/E$ %	*Number of modes to obtain 90 %*	*Number of modes to obtain 95 %*
11	0	18.5	9	13
12	0	20.8	9	13
13	10	23.8	9	13
18	15	32	9	13
15	20	28.8	9	13
20	25	25.4	10	14

	POD total energy and number of modes for the solid phase velocity $\boldsymbol{u}_s$ -Uc				*POD total energy and number of modes for the solid phase velocity $\boldsymbol{w}_s$*		
Case	Uc (cm/s)	$\lambda 1/E$ %	*Number of modes to obtain 90 %*	*Number of modes to obtain 95 %*	$\lambda 1/E$ %	*Number of modes to obtain 90 %*	*Number of modes to obtain 95 %*
11	0	43.6	4	6	40	6	7
12	0	48.5	5	6	41	6	7
13	10	40	5	7	37	6	8
18	15	31	**5**-6	**7**-8	37	8	11
15	20	39	5-6	7-8	28	8	10
20	25	42	**5-6**	**7-8**	23	9	11

Tab. 2: *POD total energy and number of modes for the solid phase fraction and solid phase velocities $\boldsymbol{u}_s$ –Uc* and $\boldsymbol{w}_s$.

About ambient current, results reported in table 2 show that this parameter has an impact on the dynamics of the flow. For $\boldsymbol{u}_s$, the increase of *Uc* leads to a rapid concentration of the total energy E towards the first mode, to reach more than 90% of E. This results support observations made about the impact of *Uc* on the spatio-temporal organization of the flow in section 5: this impact is clearly marked on $\boldsymbol{u}_s$, and more particularly on the first eigenfunction and amplitude coefficient. In an opposite way, for w_s, it can be observed an increasing of the number of modes needed to reach the same threshold.

As explained in section 5, a complementary POD decomposition was applied on $\boldsymbol{u}_s$-*Uc* snapshots, it can be observed that the eigenvalues obtained λ_i (not presented here) are exactly the same that λ_{i+1} obtained from the decomposition of $\boldsymbol{u}_s$ (cf. Figure 10). For $\boldsymbol{u}_s$-*Uc*, 90% and 95% of E are respectively reached with the 4 and 6 eigenvalues for *Uc*=0 cm/s. The increasing of *Uc* implies a progressive increase of the number of modes necessary to reach the same percentage of E : 6 and 8 for 90% and 95% (cf. Table 2).

These results support the conclusion announced in section 5 about the impact of *Uc* on the spatio-temporal organization loss.

VII. CONCLUSION AND PERSPECTIVES

Numerical simulation and POD of mud release were carried out to explore the temporal and spatial pattern and its energetical weight. In this work, cases treated correspond to some of the test conditions studied by Villaret et al. [1] by an experimental way.

The results show that a low number of eigenvalues associated to spatio-temporal modes can capture the most important characteristics of the dynamic for all the cases decomposed by POD and for solid volume fraction and solid phase velocities distributions. So, it can be inferred that POD decomposition can lead to a reduced order model via Galerkin method.

One of the parameter varying in the experiments of Villaret et al. [1] is the particle diameter. From spatio-temporal modes and energetical results extracted from cases e 11 and 12 it can be concluded that the particle diameter has not a relevant impact on the coherence of the dynamics for release without ambient current.

To estimate if the impact of *Uc* observed for *Dp*=90 µm is also shown for *Dp*=160 µm.and thus improve the comprehension of the influence of the particle diameter, it can be interesting to make complementary decompositions for sand 2 with different ambient current values.

About the impact of ambient current on solid volume phase it seem reasonably to say that the spatio-temporal organization has the same pattern in spite of the increase of Uc. Moreover this organization becomes less coherent when *Uc* increases.

Comparison of results extracted from POD applied on $\boldsymbol{u}_s$ and $\boldsymbol{u}_s$-*Uc* snapshots illustrate that the dynamic of the flow is mainly concentrated in $\boldsymbol{u}_s$ -Uc. The main modification carried out by *Uc* increasing is the loss of coherence of structures.

It can be interesting to apply a POD on vorticity snapshots which includes the contribution of the two velocity components. Indeed, this new data can let us to clarify the link between the particle dispersion and the flow dynamics. The development of this last task can be a part of a future work.

REFERENCES

1. Villaret C., Claude B., Du Rivau JD. Etude expérimentale de la dispersion des rejets par clapage. He-42/98/065/a, LNHE, EDF ; 1998.
2. Guillou S., Chauchat J., Pham Van Bang D., Nguyen DH., Nguyen KD. Simulation of the dredged sediment's release with a two-phase flow model, Bulletin of the Permanent International Association of Navigation Congresses 2011; 142: 25-33, ISSN 0374-1001.
3. Barbry N., Guillou S., Nguyen KD. Une approche diphasique pour le calcul du transport sédimentaire en milieux estuariens. C.R. Acad. Sci., IIb 2000; 328: 793–799.
4. Nguyen KD., Guillou S., Chauchat J., Barbry N. A two-phase numerical model for suspended-sediment transport in estuaries. Advances in Water Resources 2009; 32: 1187-1196.
5. Nguyen DH., Guillou S., Nguyen KD., Pham Van Bang D., Chauchat J. Two-Dimensional simulations of dredged sediment release with a two-phase model, THESIS 2011; 4p.
6. Holmes P., Lumley JL., and Berkooz G. Turbulence, coherent structures, dynamical systems, and symmetry. Cambridge University Press 1996.
7. Sirovich L. Turbulence and the dynamics of coherent structures. Quarterly of Applied Mathematics 1987; 5: 561-590.
8. Cizmas PG., Palacios A., O'Brien T., Syamlal M. Proper-orthogonal decomposition of spatio-temporal patterns in fluidized beds, Chemical Engineering Science 2003; 58: 4417–4427.
9. Yuan T., Cizmas PG., O'Brien TO. A reduced model for a bubbling fluidized bed based on proper orthogonal decomposition, Computer & chemical engineering 2005; 30: 243-259.
10. Brenner TA., Fontenot RL., Cizmas PG., O'Brien TO., Breault RW. Augmented proper orthogonal decomposition for problems with moving discontinuities, Powder technology 2010; 203: 78-85.